Coupled Orbit–Attitude Dynamics and Relative State Estimation of Spacecraft near Small Solar System Bodies

Article *in* Advances in Space Research · May 2015

DOI: 10.1016/j.asr.2015.05.023

CITATIONS
56

READS
330

4 authors, including:

Gaurav Misra
Rutgers, The State University of New Jersey
22 PUBLICATIONS **159** CITATIONS
SEE PROFILE

Sanyal Amit
Syracuse University
161 PUBLICATIONS **2,690** CITATIONS
SEE PROFILE

D. J. Scheeres
University of Colorado Boulder
952 PUBLICATIONS **18,989** CITATIONS
SEE PROFILE

Coupled Orbit-Attitude Dynamics and Relative State Estimation of Spacecraft near Small Solar System Bodies

Gaurav Misra[1], Maziar Izadi[1], Amit Sanyal[2,*]

Department of Mechanical and Aerospace Engineering, New Mexico State University, Las Cruces, NM 88003, United States

Daniel Scheeres[3]

Aerospace Engineering Sciences, University of Colorado, Boulder, CO 80309, United States

Abstract

The effects of dynamical coupling between the rotational (attitude) and translational (orbital) motion of spacecraft near small Solar System bodies is investigated. This coupling arises due to the weak gravity of these bodies, as well as solar radiation pressure. The traditional approach assumes a point-mass spacecraft model to describe the translational motion of the spacecraft, while the attitude motion is considered to be completely decoupled from the translational motion. The model used here to describe the rigid-body spacecraft dynamics includes the non-uniform rotating gravity field of the small body up to second degree and order along with the attitude dependent terms, solar tide, and solar radiation pressure. This model shows that the second degree and order gravity terms due to the small body affect the dynamics of the spacecraft to the same extent as the orbit-attitude coupling due to the primary gravity (zeroth order) term. Variational integrators are used to simulate the dynamics of both the rigid spacecraft and the point mass. The small bodies considered here are modeled after Near-Earth Objects (NEO)

*Corresponding author

Email address: asanyal@nmsu.edu (Amit Sanyal)

[1]Graduate Student

[2]Assistant Professor

[3]Professor

101955 Bennu, and 25143 Itokawa, and are assumed to be triaxial ellipsoids with uniform density. Differences in the numerically obtained trajectories of a rigid spacecraft and a point mass are then compared, to illustrate the impact of the orbit-attitude coupling on spacecraft dynamics in proximity of small bodies. Possible implications on the performance of model-based spacecraft control and on the station-keeping budget, if the orbit-attitude coupling is not accounted for in the model of the dynamics, are also discussed. An almost globally asymptotically stable motion estimation scheme based solely on visual/optical feedback that estimates the relative motion of the asteroid with respect to the spacecraft is also obtained. This estimation scheme does not require a model of the dynamics of the asteroid, which makes it perfectly suited for asteroids whose properties are not well known.

Keywords: Orbit-Attitude Coupling; Relative Pose Estimation; Small Bodies

1. Introduction

The dynamics and control of spacecraft in proximity to asteroids and comets has been a topic of research interest in recent times. Missions such as NEAR Shoemaker (Miller et al., 2002), Hayabusa (Fujiwara et al., 2006), and Dawn (Russell et al., 2012) have demonstrated the ability to perform close-proximity operations near small bodies. The dynamical environment near these small bodies has unique complexities. This is primarily due to the weak and non-uniform rotating gravity field that arises from the irregular shape, non-homogeneous mass distribution, and rotation of the small body. In addition, strong perturbations due to solar radiation pressure and third-body gravitational effects pose challenges for small body proximity operations (Scheeres, 2012a). Several studies have dealt with the dynamics of spacecraft near small bodies, within the traditional framework that models the spacecraft as a point mass for its motion around the small body (Scheeres, 1994; Hu, 2002; Hu and Scheeres, 2002; Yu and Baoyin, 2012). Based on this framework, a number of approaches for close-proximity operations have been considered. These include direct orbits, retrograde orbits, and terminator orbits under the general setting of bounded orbital motion; other approaches that have been explored include controlled hovering (Broschart, 2006), and close flybys (Takahashi and Scheeres, 2011).

An important aspect of the dynamics of spacecraft near small Solar Sys-

tem bodies that has direct implications on missions exploring these bodies, is the coupling between the rotational and translational motion of the spacecraft. This coupling is induced by the weak gravity of the small body on the spacecraft, as well as perturbations like solar radiation pressure (Sincarsin and Hughes, 1983). The magnitude of this coupling depends on the spacecraft mass distribution, its orientation and size relative to its orbit. Sincarsin and Hughes (1983) describe the effect of orbit-attitude coupling by expanding the differential gravitational force and torque in a Taylor series in the parameter $\epsilon = \frac{\rho}{r}$, where ρ is the characteristic spacecraft size and r is the orbit radius. For Earth missions, as the orbit radius is much larger than the spacecraft, ϵ is small and this coupling is weak and can be neglected in an analysis of the spacecraft's attitude and orbit dynamics and control (Beck and Hall, 1998). The orbital radius for small body missions is much smaller, leading to much larger values for ϵ; the effects of attitude-orbit coupling cannot in general be ignored for small body proximity missions. Some space agencies have announced plans for future small body exploration and hazard mitigation missions (Mazanek et al., 2013; Tsuda et al., 2013; Harris et al., 2013). Asteroid hazard mitigation techniques include gravity tractors (Lu and Love, 2005), laser ablation (Vasile and Maddock, 2012), and solar sails (Prado et al., 2011). All such missions will require spacecraft that have large ϵ in proximity operations around small bodies; therefore it will be essential to account for orbit-attitude coupling. The attitude-orbit coupling will also have a crucial impact on the recently announced Asteroid Retrieval Mission (ARM) (Mazanek et al., 2013), where the size of the exploring spacecraft is comparable to the small asteroid. Mohan et al. (1972) and Pascal (1985) have studied attitude-orbit coupling for Earth orbiting spacecraft. Sanyal (2004) studied the coupled dynamics in context of multibody systems in a central gravitational field, and its uses for the design of new control techniques. Attitude-orbit coupling has also been studied in the context of spacecraft formation flying (Segal and Gurfil, 2009; Pan and Kapila, 2001), and space debris (Fruh et al., 2013). Koon et al. (2004); Scheeres et al. (2006) studied coupled orbit-attitude dynamics for natural systems, such as the full two body problem of binary asteroids. However, this coupling has not been considered important in the context of spacecraft missions exploring small bodies.

This study focuses on the effects of attitude-orbit coupling for spacecraft operating in proximity to small Solar System bodies. In particular, it looks at the trajectories obtained for rigid body spacecraft, for initial states of the

spacecraft that are known to lead to stable trajectories for a point mass. As has been shown in prior research, frozen terminator orbits are one of the ballistic orbit classes that exhibit long-term stable behavior under solar radiation pressure effects. Scheeres (1999) computed frozen orbit solutions for a point mass as a result of the averaged effects of solar radiation pressure (using a flat plate model) based on results by Mignard and Hènon (1984). Two families of orbits that maintain a fixed orientation relative to the solar radiation pressure direction as the small body moves in an elliptical orbit were found. These two families of orbits are designated as: (1) frozen terminator orbits, also known as solar Plane-of-Sky frozen orbits, wherein the spacecraft orbits in a plane perpendicular to the Sun-asteroid line with the angular momentum vector either pointing towards or away from the Sun; and (2) frozen ecliptic orbits, wherein the spacecraft orbits the asteroid in the orbital plane of the asteroid with the periapse vector pointing either towards or away from the Sun. Amongst these orbits, frozen terminator orbits are planned to be used by the upcoming OSIRIS-REx mission (Scheeres et al., 2013).

Given that such orbits constitute the proposed solutions for small body missions, it is important to analyze the effects that could pose challenges to their implementation. Sections 2 and 3 describe the dynamics of the asteroid and spacecraft respectively, with both rigid-body and point-mass models of the spacecraft presented in Section 3. Section 4 discretizes the dynamics of the rigid body spacecraft in the form of a Lie group variational integrator for a non-conservative system (e.g., Nordkvist and Sanyal (2010); Lee et al. (2007)). This is followed by numerical simulations for various test cases in Section 5, where the effects of attitude-orbit coupling on the trajectory of the rigid body spacecraft are shown. We use the analytical methodology proposed by Scheeres (1999) to find initial orbital elements for frozen terminator orbits for our numerical simulations around asteroid 101955 Bennu. In addition, we also show numerical simulations around asteroid 25143 Itokawa, using random initial conditions, with and without the inclusion of solar radiation pressure. The implications of the dynamic coupling on mission lifetime, payload and stationkeeping budget are then presented in Section 6, followed by a discussion on utilizing the coupled dynamics for small-body exploration rather than mitigating such effects using controls. During small-body proximity operations, the relative pose and velocities of the body with respect to the spacecraft can be estimated using range and perhaps range-rate measurements. Preliminary results on relative motion (pose and velocities) estimation from visual feedback, based on the Lagrange-d'Alembert principle

applied to a Lagrangian constructed from estimation errors with a Rayleigh dissipation term, were presented by Sanyal et al. (2014b). This technique was previously used to derive an estimator for attitude (Izadi and Sanyal, 2014). A relative pose and velocity estimation scheme based on this technique is presented in Section 7. This estimator uses vision-based measurements, without needing a model of the dynamics of the observed small body. The proof of stability and domain of attraction of this estimator are also presented.

2. Asteroid Dynamics

The asteroid is modeled as a rigid body that orbits the Sun under the influence of its central gravity field. There are three coordinate frames used in this study, a heliocentric inertial frame, an asteroid body-fixed frame centered in its center of mass, and a spacecraft body-fixed frame centered in its center of mass. The configuration space of the asteroid is the special Euclidean group SE(3), which is the set of all translational and rotational motions of a rigid body. SE(3) is also a Lie group and can be expressed as the semi-direct product $\mathrm{SE}(3) = \mathbb{R}^3 \ltimes \mathrm{SO}(3)$, where $\mathbb{R}^3$ is the three-dimensional real Euclidean space of positions of the center of mass of the body, and SO(3) is the Lie group of orientations of the rigid body. A superscript$(\cdot)^0$ is used to specify the asteroid states and parameters. The asteroid attitude is represented by the rotation matrix $R^0 \in \mathrm{SO}(3)$ that transforms a vector from the asteroid body-fixed frame to the inertial frame. The asteroid's position is expressed by the inertial position vector $b^0 \in \mathbb{R}^3$ from the origin of the heliocentric inertial frame to the center of the mass of the asteroid. Translational and angular velocities of the asteroid are expressed by the vectors $\nu^0 \in \mathbb{R}^3$ and $\Omega^0 \in \mathbb{R}^3$, respectively, expressed in the asteroid body-fixed frame. The coordinate frames and position vectors associated with the motion of the asteroid and the spacecraft are depicted in Figure 1.

The kinematics of the asteroid is expressed as

$$\dot{b}^0 = R^0\nu^0, \ \dot{R}^0 = R^0(\Omega^0)^\times, \tag{1}$$

where $(\cdot)^\times : \mathbb{R}^3 \to \mathfrak{so}(3)$ denotes the cross-product operator defined by

$$v^\times = \begin{bmatrix} v_1 \\ v_2 \\ v_3 \end{bmatrix}^\times = \begin{bmatrix} 0 & -v_3 & v_2 \\ v_3 & 0 & -v_1 \\ -v_2 & v_1 & 0 \end{bmatrix}.$$

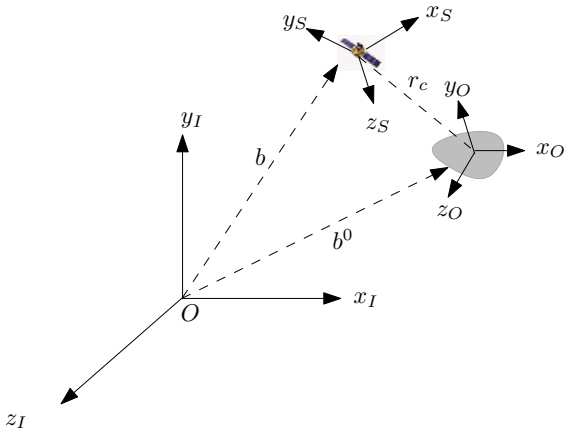

Figure 1: Coordinate frames and position vectors (not to scale) associated with the motion of the asteroid and the spacecraft.

Here, $\mathfrak{so}(3)$ is the Lie algebra of SO(3), which is represented as the linear space of 3×3 skew-symmetric matrices. Let the asteroid's mass be chosen as m^0 and its inertia matrix be J^0 in its body frame. The dynamics of the asteroid are given by

$$m^0 \dot{\nu}^0 = m^0 \nu^0 \times \Omega^0 + F_g^0(b^0, R^0), \tag{2}$$

$$J^0 \dot{\Omega}^0 = J^0 \Omega^0 \times \Omega^0 + M_g^0(b^0, R^0), \tag{3}$$

where $F_g^0, M_g^0 \in \mathbb{R}^3$ denote the gravity force (Schaub and Junkins, 2009) and gravity gradient moment (both expressed in the asteroid body-fixed frame) on the asteroid due to the Sun, respectively, as given by

$$F_g^0 = -\left(\frac{m^0 \mu_S}{\|b^0\|^3}\right) p^0 - 3\left(\frac{\mu_S}{\|b^0\|^5}\right) \mathcal{J}^0 p^0 + \frac{15}{2} \left(\frac{\mu_S (p^{0\mathrm{T}} J^0 p^0)}{\|b^0\|^7} \right) p^0, \tag{4}$$

$$M_g^0 = 3 \left(\frac{\mu_S}{\|b^0\|^5} \right) (p^0 \times J^0 p^0), \tag{5}$$

where $p^0 = (R^0)^{\mathrm{T}} b^0$, $\mathcal{J}^0 = \frac{1}{2}\mathrm{tr}(J^0) I + J^0$, and μ_S is the gravitational parameter of the Sun. The state space of the asteroid is $\mathrm{TSE}(3) \simeq \mathrm{SE}(3) \times \mathfrak{se}(3)$ and its motion states are denoted by $(b^0, R^0, \nu^0, \Omega^0)$. Here $\mathfrak{se}(3)$ denotes the Lie algebra (tangent space at the identity) of the Lie group SE(3), and $\mathfrak{se}(3)$ is isomorphic to $\mathbb{R}^6$ as a vector space.

3. Spacecraft Dynamics

3.1. Solar Radiation Pressure

One of the most important non-gravitational perturbations is Solar radiation pressure (SRP). In small-body missions, the force is strong enough to cause a spacecraft to impact or be ejected from the small body vicinity.

3.1.1. Flat Plate Model

In most preliminary mission designs, SRP is modeled assuming a two-dimensional, flat-plate model of the spacecraft. Using this assumption, the magnitude of the acceleration due to SRP is given as (Giancotti, 2014)

$$a = \frac{L_\odot(1+\rho)}{4\pi c b^2 B}, \tag{6}$$

where $\rho \in [0,1]$ is the reflectivity parameter of the spacecraft, B is the spacecraft mass to area ratio, c is the speed of light, b is the distance of the spacecraft from the Sun, and $L_\odot$ is the solar luminosity. The direction of the SRP acceleration is dependent on the angle between the incident light ($\hat{l}$) and the normal ($\hat{n}$) to the body's surface. The acceleration for a perfectly reflecting body ($\rho = 1$) can be written as

$$a_{srp} = -a(\hat{l}\cdot\hat{n})^2\hat{n}. \tag{7}$$

3.1.2. Cuboid Shape Model

In this study, a cuboidal shape model is considered for the spacecraft. The expression for SRP acceleration is given as

$$a^B_{srp} = -\frac{P_0}{mcb^2}\sum_{i=1}^{6} A_i\lambda_i^2 u_{srp_i}, \tag{8}$$

where

$$u_{srp_i} = 2\left[\frac{R_{diff}}{3} + \frac{\epsilon R_{abs}}{3} + R_{spec}\lambda_i\right]\hat{n_i} + \left[1 - R_{spec}\right]\hat{l^B}, \tag{9}$$

$$\lambda_i = max\left[0, \hat{l^B}^T\cdot\hat{n_i}\right]. \tag{10}$$

where m is the total mass of the spacecraft, P_0 is the mean solar flux at 1 AU, b is the spacecraft distance from the Sun in AU; ϵ, R_{diff}, R_{abs}, and R_{spec}

are the emmisivity, diffuse reflectance, absorption and specular reflectance coefficients respectively. $\hat{l}^B$ is the unit vector to the Sun in the spacecraft body frame, and $\hat{n}$ is the unit outward normal for the i-th plate of the cuboid spacecraft in its body frame. The expression for the torque produced due to SRP in the spacecraft body frame is formulated as

$$\tau_{srp} = m \sum_{i=1}^{6} \xi_i^B \times a_{srp_i}^B. \tag{11}$$

where ξ_i^B is the centroid location for each plate of the spacecraft expressed in its body frame, and $a_{srp_i}^B$ is the acceleration due to SRP for each plate expressed in the spacecraft body frame.

3.2. Rigid body model

The configuration of the spacecraft modeled as a rigid body is given by the position vector from the origin of the heliocentric inertial frame to the center of mass of the spacecraft (denoted by $b \in \mathbb{R}^3$), and the attitude given by the rotation matrix from a body-fixed coordinate frame to the heliocentric inertial frame (denoted $R \in \mathrm{SO}(3)$). The kinematics for the spacecraft takes the same form as the kinematics for the asteroid, and is given by

$$\dot{b} = R\nu, \;\; \dot{R} = R\Omega^{\times}, \tag{12}$$

where $\nu \in \mathbb{R}^3$ is the translational velocity, and $\Omega \in \mathbb{R}^3$ is the angular velocity of the spacecraft, both vectors being expressed in the spacecraft's body frame. The state space for the spacecraft's motion is $\mathrm{SE}(3) \times \mathfrak{se}(3)$.

Let the spacecraft mass be denoted m and its inertia matrix be J in its body-fixed frame. The equations of motion for the rigid body spacecraft without any control inputs are therefore given as follows

$$m\dot{\nu} = m\nu \times \Omega + F_{g_{S-c}}(b, R) + F_{srp}(b, R) + F_{g_{a-c}}(r_c, \bar{R}), \tag{13}$$

$$J\dot{\Omega} = J\Omega \times \Omega + M_{g_{S-c}}(b, R) + \tau_{srp}(b, R) + M_{g_{a-c}}(r_c, \bar{R}), \tag{14}$$

where $F_{g_{S-c}}$, $M_{g_{S-c}} \in \mathbb{R}^3$ denote the gravity force, and gravity gradient moment due to the Sun, F_{srp}, $\tau_{srp} \in \mathbb{R}^3$ denote the force and moment due to SRP on the spacecraft, respectively, and $F_{g_{a-c}}$, $M_{g_{a-c}} \in \mathbb{R}^3$ denote the gravity force, and gravity gradient moment on the spacecraft due to the asteroid, respectively, $r = [x \;\; y \;\; z]^{\mathrm{T}}$ is the relative position vector of

an arbitrary point on the spacecraft in the asteroid body-fixed frame, $r_c = [x_c \ y_c \ z_c]^{\mathrm{T}}$ is the relative position vector of the center of the mass of the spacecraft in the asteroid body-fixed frame, and $\bar{R} = R^{\mathrm{T}} R^0$ is the rotation matrix that transforms from the asteroid body-fixed frame to the spacecraft body-fixed frame. The gravity force and gradient moment on the spacecraft due to the Sun have the same form as the gravity force and gradient moment on the asteroid, which are given by eq (4)-(5). The gravity force on the spacecraft by the asteroid $F_{g_{a-c}}$ is described using the second degree and order spherical harmonic gravity field in the asteroid body-fixed frame. The origin of the asteroid body-fixed coordinate system is assumed to coincide with the center of mass of the asteroid, thereby rendering the first degree, and order gravity terms zero, $C_{11} = C_{10} = S_{11} = 0$. Furthermore, since the small bodies in this study are modeled as triaxial ellipsoids with homogeneous density, the second degree and order terms C_{21}, S_{21}, S_{22} are also identically zero (Scheeres, 2012b); note that this is true even if the coordinate frame fixed to the small body is the principal axes frame. The gravity potential of second degree and order in the asteroid body-fixed frame (Scheeres, 2012b) is

$$U_{2a} = -\frac{\mu_a C_{20}(x^2 + y^2 - 2z^2)}{2\|r\|^5} + \frac{3\mu_a C_{22}(x^2 - y^2)}{\|r\|^5}, \tag{15}$$

where μ_a is the gravitational parameter of the asteroid, $\|r\| = \sqrt{(x^2 + y^2 + z^2)}$, and C_{20} and C_{22} are the second degree and order gravity coefficients. The effective gravity potential function of the asteroid is

$$U_a = \frac{\mu_a}{\|r\|} + U_{2a} = \frac{\mu_a}{\|r\|} - \frac{\mu_a C_{20}(x^2 + y^2 - 2z^2)}{2\|r\|^5} + \frac{3\mu_a C_{22}(x^2 - y^2)}{\|r\|^5}. \tag{16}$$

The first-order partial derivatives of the effective gravity potential U in

eq (16) with respect to x, y and z are

$$\begin{aligned}\frac{\partial U}{\partial x} =& -\frac{\mu_a x}{\|r\|^3} - \frac{\mu_a C_{20} x}{\|r\|^5} + \frac{5\mu_a C_{20} x(x^2+y^2-2z^2)}{2\|r\|^7} + \frac{6\mu_a C_{22} x}{\|r\|^5} \\ & - \frac{15\mu_a C_{22} x(x^2-y^2)}{\|r\|^7}, \end{aligned} \tag{17}$$

$$\begin{aligned}\frac{\partial U}{\partial y} =& -\frac{\mu_a y}{\|r\|^3} - \frac{\mu_a C_{20} y}{\|r\|^5} + \frac{5\mu_a C_{20} y(x^2+y^2-2z^2)}{2\|r\|^7} - \frac{6\mu_a C_{22} y}{\|r\|^5} \\ & - \frac{15\mu_a C_{22} y(x^2-y^2)}{\|r\|^7}, \end{aligned} \tag{18}$$

$$\frac{\partial U}{\partial z} = -\frac{\mu_a z}{\|r\|^3} + \frac{2\mu_a C_{20} z}{\|r\|^5} + \frac{5\mu_a C_{20} z(x^2+y^2-2z^2)}{2\|r\|^7} - \frac{15\mu_a C_{22} z(x^2-y^2)}{\|r\|^7}. \tag{19}$$

The first-order partial derivatives of the effective gravity potential U in eq(16) about the relative position vectors r and r_c are:

$$\frac{\partial U}{\partial r} = \begin{bmatrix}\frac{\partial U}{\partial x} & \frac{\partial U}{\partial y} & \frac{\partial U}{\partial z}\end{bmatrix}^{\mathrm{T}}. \tag{20}$$

The gravity force due to the effective gravity potential U of the asteroid in eq. (16) in the asteroid body-fixed frame is:

$$F^0_{g_{a-c}} = \int \frac{\partial U}{\partial r} dm. \tag{21}$$

Using the rotation matrix $\bar{R} = R^{\mathrm{T}} R^0$ that transforms to the spacecraft body-fixed frame from the asteroid body-fixed frame, the gravity force due to the gravity potential in eq. (16) in the spacecraft body-fixed frame is expressed by

$$F_{g_{a-c}} = R^{\mathrm{T}} R^0 \int \frac{\partial U}{\partial r} dm = \bar{R} F^0_{g_{a-c}}. \tag{22}$$

The integration of the first columns in eqs. (17) (18), and (19) as the vector form denoted by $F^p_{g_{a-c}}$ is the primary gravity force term:

$$F^p_{g_{a-c}} = \bar{R} \int \frac{-\mu_a}{\|r\|^3}\, r\, dm = -\frac{m\mu_a}{\|r_c\|^3} p_c - 3\Big(\frac{\mu_a}{\|r_c\|^5}\Big)\mathcal{J} p_c + \frac{15}{2}\left(\frac{\mu_a (p_c^{\mathrm{T}} J p_c)}{\|r_c\|^7}\right) p_c. \tag{23}$$

where $p_c = \bar{R}r_c = [\bar{x}_c \ \bar{y}_c \ \bar{z}_c]^{\mathrm{T}}$ which is the relative position vector of the center of mass of the spacecraft in the spacecraft body-fixed frame, and $\mathcal{J} = \frac{1}{2}\mathrm{tr}(J)I + J$. In the subsequent analysis of the translational and orbital dynamics of the spacecraft, only the terms up to order $\|r\|^{-4}$ are included in approximations of the gravity force and gravity gradient moment due to the asteroid on the spacecraft. This, incidentally, includes the terms dependent on C_{20} and C_{22} in the approximation of the gravity force, but excludes these terms in the approximation of the gravity gradient moment on the spacecraft due to the asteroid. Thus, the gravity force due to the gravity potential in eq. (16) in the spacecraft body-fixed frame is approximated as follows:

$$F_{g_{a-c}} = F^{p}_{g_{a-c}} + \ \bar{R}F^{2}_{g_{a-c}} = -\frac{m\mu_a}{\|r_c\|^3}p_c - 3\Big(\frac{\mu_a}{\|r_c\|^5}\Big)\mathcal{J}p_c + \frac{15}{2}\left(\frac{\mu_a(p_c^{\mathrm{T}}Jp_c)}{\|r_c\|^7}\right)p_c + \bar{R}F^{2}_{g_{a-c}}, \tag{24}$$

where

$$F^{2}_{g_{a-c}} = m\left\{\begin{array}{l} -\frac{\mu_a C_{20}x_c}{\|r_c\|^5} + \frac{5\mu_a C_{20}x_c(x_c^2+y_c^2-2z_c^2)}{2\|r_c\|^7} + \frac{6\mu_a C_{22}x_c}{\|r_c\|^5} - \frac{15\mu_a C_{22}x_c(x_c^2-y_c^2)}{\|r_c\|^7} \\ -\frac{\mu_a C_{20}y_c}{\|r_c\|^5} + \frac{5\mu_a C_{20}y_c(x_c^2+y_c^2-2z_c^2)}{2\|r_c\|^7} - \frac{6\mu_a C_{22}y_c}{\|r_c\|^5} - \frac{15\mu_a C_{22}y_c(x_c^2-y_c^2)}{\|r_c\|^7} \\ \frac{2\mu_a C_{20}z_c}{\|r_c\|^5} + \frac{5\mu_a C_{20}z_c(x_c^2+y_c^2-2z_c^2)}{2\|r_c\|^7} - \frac{15\mu_a C_{22}z_c(x_c^2-y_c^2)}{\|r_c\|^7} \end{array}\right\}.$$

In addition, the gravity-gradient moment on the spacecraft due to this approximation has the same form as the gravity-gradient moment due to the Sun on the asteroid, which is given by

$$M_{g_{a-c}} = 3\left(\frac{\mu_a}{\|r_c\|^5}\right)(p_c \times Jp_c). \tag{25}$$

The gravity force terms dependent on C_{20} and C_{22} are of the order of $\|r_c\|^{-4}$, while the primary gravity force term is of the order of $\|r_c\|^{-2}$. It is interesting to note that the gravity force from the orbit-attitude coupling due to the primary gravity term, given by the last two terms on the right side of eq. (24), is also of order $\|r_c\|^{-4}$. Therefore, the orbit-attitude coupling has the same order effect on the gravity force acting on the spacecraft as the higher-order gravity potential terms containing C_{20} and C_{22}.

3.3. Point mass model

Let the inertial position and velocity states of a point mass in the vicinity of the asteroid be represented by b_p and $\dot{b}_p$, respectively, while its position

with respect to the asteroid-fixed frame is denoted $r_{c,p}$. The dynamics for a point mass without control inputs and acted on by the gravity of the Sun and the asteroid is represented in the inertial frame as

$$\ddot{b}_p = -\frac{\mu_S}{\|b_p\|^3} b_p - \frac{\mu_a}{\|r_{c,p}\|^3} r_{c,p} + \frac{\partial U_2}{\partial r_{c,p}} + F_{srp}(b_p). \tag{26}$$

In order to simulate the point mass spacecraft dynamics, we use a Störmer-Verlet method (Hairer et al., 2002). The method is variational (symplectic in the absence of SRP) and preserves the geometry of the phase space.

4. Discretization of Dynamics Models

The dynamics of the asteroid and spacecraft, both modeled as rigid bodies, are discretized using a Lie group variational integrator (LGVI) (Lee et al., 2007). A variational integrator works by discretizing the (continuous-time) variational mechanics principle that leads to the equations of motion, rather than discretizing the equations of motion directly. A good background on variational integrators is given in the excellent treatise by Marsden and West (2001). The correspondence between variational integrators and symplectic integrators (for conservative systems) is given in the book by Hairer et al. (2002). LGVIs are variational integrators for mechanical systems whose configuration spaces are Lie groups, like rigid body systems. In addition to maintaining properties arising from the variational principles of mechanics, like energy and momenta, LGVI schemes also maintain the geometry of the Lie group that is the configuration space of the system (Lee et al., 2007). Such schemes have also been developed and used to numerically simulate the dynamics of rigid bodies in the presence of non-conservative forces and torques (Nordkvist and Sanyal, 2010; Lee et al., 2007; Hussein et al., 2006). The Lagrangian for the motion of a rigid body in SE(3) is given by

$$\mathcal{L}(b, \nu, R, \Omega) = \frac{1}{2} \langle J\Omega, \Omega \rangle + \frac{1}{2} \langle M\nu, \nu \rangle - U(b, R) \tag{27}$$

where the inner product $\langle A, B \rangle := tr(A^{\mathrm{T}} B)$. The dynamics of the system satisfies the (continuous) Lagrange-d'Alembert principle (Marsden and West, 2001)

$$\delta \int_{t_0}^{T} \mathcal{L}(b, \nu, R, \Omega) + \int_{t_0}^{T} ((\tau, \Sigma) + (\varphi, \gamma)) = 0 \tag{28}$$

where τ, and φ denote the nonconservative moment and forces, in the body frame. According to Marsden and Ratiu (1999), the infinitesimal variations δb, $\delta\nu$, δR, and $\delta\Omega$ satisfy

$$\begin{aligned} \delta b &= R\gamma, \\ \delta\nu &= \dot{\gamma} + \Omega^{\times}\gamma + \nu^{\times}\Sigma, \\ \delta R &= R\Sigma^{\times}, \\ \delta\Omega &= \dot{\Sigma} + \Omega^{\times}\Sigma, \end{aligned} \tag{29}$$

where Σ and γ vanish at the end points but are otherwise arbitrary.

4.1. Discrete Variational Mechanics for Rigid Body Motion

A variational integrator discretizes Hamilton's principle or the Lagrange-d'Alembert principle, rather than directly discretizing the continuous equations of motion. As a first step in obtaining the LGVI that discretizes the dynamics in eqs. (2)-(3) and (13)-(14), a discrete-time counterpart of the (continuous-time) Lagrangians corresponding to these dynamics is obtained.

Let f_k denote the discrete approximation to a continuous time-varying quantity f at time $t_k = t(k)$. Denote by $h \neq 0$ the fixed time-step size, i.e., $t_{k+1} - t_k = h$. Consider discretization of the dynamics of the rigid body spacecraft: the *discrete Lagrangian* $\mathcal{L}_d$ approximates a segment of the action integral

$$\mathcal{L}_d(b_k, \nu_k, R_k, \Omega_k) \approx \int_{t_k}^{t_{k+1}} \mathcal{L}(b, \nu, R, \Omega)dt. \tag{30}$$

Similarly, we construct $\mathcal{F}$ to approximate a segment of the virtual work integral

$$\begin{aligned} \mathcal{F}_k &\approx \int_{t_k}^{t_{k+1}} (\langle \tau, \Sigma \rangle + \langle R\varphi, \delta b \rangle)dt \\ &= \int_{t_k}^{t_{k+1}} (\frac{1}{2}\left\langle \tau^{\times}, \Sigma^{\times} \right\rangle + \langle \varphi, \gamma \rangle)dt. \end{aligned} \tag{31}$$

where we have used $\langle a, b \rangle = \frac{1}{2}\left\langle a^{\times}, b^{\times} \right\rangle$ for a, b $\in \mathbb{R}^3$. The discrete dynamics is then obtained by applying the *discrete Lagrange-d'Alembert principle* (Monforte, 2002)

$$\delta \sum_{k=0}^{N-1} \mathcal{L}_d(b_k, \nu_k, R_k, \Omega_k) + \sum_{k=0}^{N-1} \mathcal{F}_k = 0, \tag{32}$$

where $\Sigma_0 = \Sigma_N = 0$ and $\gamma_0 = \gamma_N = 0$.

4.2. Discrete Equations of Motion

Discretizing the kinematics (12) with the assumption of constant angular velocity in the time interval $[t_k, t_{k+1}]$, one obtains

$$R_{k+1} = R_k F_k, \tag{33}$$

where $F_k \in \mathrm{SO}(3)$ is given by

$$F_k = \exp(h\Omega_k^\times) \approx I + h\Omega_k^\times. \tag{34}$$

This guarantees that R_k evolves on SO(3). Skew symmetry of $\Omega_k^\times$ is ensured by:

$$\begin{aligned}(J\Omega_k)^\times &= \Omega_k^\times \mathcal{J} - \mathcal{J}(\Omega_k^\times)^{\mathrm{T}} \approx \frac{1}{h}\Big((F_k - I)\mathcal{J} - \mathcal{J}(F_k^{\mathrm{T}} - I)\Big) \\ &= \frac{1}{h}(F_k\mathcal{J} - \mathcal{J}F_k^{\mathrm{T}}) \text{ where } \mathcal{J} = \frac{1}{2}\mathrm{tr}(J)I - J.\end{aligned} \tag{35}$$

From (12), the discrete kinematics for b_k assuming constant velocity ν_k in the time interval $[t_k, t_{k+1}]$, is given by

$$b_{k+1} = hR_k\nu_k + b_k. \tag{36}$$

Hence the discrete counterpart of the kinematic equations (12) is

$$(J\Omega_k)^\times = \frac{1}{h}(F_k\mathcal{J} - \mathcal{J}F_k^{\mathrm{T}}), \tag{37}$$

$$R_{k+1} = R_k F_k, \tag{38}$$

$$b_{k+1} = hR_k\nu_k + b_k. \tag{39}$$

Equation (37) can be solved for F_k given Ω_k using Newton-Raphson iterations.

The discrete Lagrangian is obtained as:

$$\begin{aligned}\mathcal{L}_d(b_k, \nu_k, R_k^0, R_k, F_k) = \frac{h}{2}\langle m\nu_k, \nu_k\rangle + \frac{h}{2}\left\langle \frac{1}{h}\mathcal{J}(F_k - I), \frac{1}{h}(F_k - I)\right\rangle \\ - \frac{h}{2}\Big(U_S(b_k, R_k) + U_S(b_{k+1}, R_{k+1})\Big) \\ - \frac{h}{2}\Big(U_a(r_k, \bar{R}_k) + U_a(r_{k+1}, \bar{R}_{k+1})\Big),\end{aligned} \tag{40}$$

where U_S and U_a denote the gravity potentials due to the Sun and the asteroid, respectively. Applying the discrete Lagrange-d'Alembert principle (32) with *reduced variations* for $F_k \in \mathrm{SO}(3)$, this leads to the discrete dynamics equations

$$\begin{aligned} m\nu_{k+1} = mF_k^{\mathrm{T}}\nu_k - hR_{k+1}^{\mathrm{T}}\frac{\partial U_S}{\partial b}(b_{k+1}, R_{k+1}) - h\bar{R}_{k+1}^{\mathrm{T}}\frac{\partial U_a}{\partial r}(r_{k+1}, \bar{R}_{k+1}) \\ + hma_{srp}^{B}(b_{k+1}, R_{k+1}) \end{aligned} \tag{41}$$

$$J\Omega_{k+1} = F_k^{\mathrm{T}} J\Omega_k + h\mathcal{U}_S(b_{k+1}, R_{k+1}) + h\mathcal{U}_a(r_{k+1}, \bar{R}_{k+1}) + \tau_{srp}^{B}(b_{k+1}, R_{k+1}), \tag{42}$$

where $\mathcal{U}(b, R) \in \mathbb{R}^3$ is defined by

$$\mathcal{U}(b, R)^{\times} = \frac{\partial U(b, R)}{\partial R}^{\mathrm{T}} R - R^{\mathrm{T}}\frac{\partial U(b, R)}{\partial R}.$$

eq (37)-(39) and (41)-(42) constitute the LGVI, which gives a one-step numerical integration scheme to numerically simulate the dynamics of the spacecraft. A similar LGVI is obtained for the asteroid's motion, with the additional simplification that only the Sun's gravity potential is considered to act on the asteroid.

5. Numerical Results

5.1. Frozen Terminator Orbit Design

We recall the established results for frozen terminator orbit design given by Scheeres (1999), and Scheeres et al. (2013). The upper bound on the initial semi-major axis of the spacecraft orbit around a small asteroid is given as (Scheeres et al., 2013)

$$a < \frac{\sqrt{3}}{4}\frac{\mu_a}{\alpha_{SRP}}, \tag{43}$$

where α_{SRP} is defined by

$$\alpha_{SRP} = \frac{(1+\rho)P_0}{Bd^2}, \tag{44}$$

where μ_a is the asteroid's gravitational parameter, ρ is the reflectance of the spacecraft, $P_0 \sim 1 \times 10^8$ kg/km^3/s^2/m^2 is the solar flux, B is the spacecraft's mass to area ratio, d is the asteroid's distance from the Sun. The expression for the eccentricity of the spacecraft orbit is

$$e = \cos \Lambda, \tag{45}$$

$$\Lambda = \tan^{-1} \big(\frac{3(1+\rho)P_0}{2B} \sqrt{\frac{a}{\mu_s \mu A (1-E^2)}} \big), \tag{46}$$

where μ_s is the gravitational parameter of the Sun. A, and E are the semi-major axis and eccentricity of the asteroid's heliocentric orbit, respectively.

5.2. Case I: 101955 Bennu

The initial heliocentric position for asteroid Bennu is taken at its perihelion. The asteroid is assumed to rotate about its maximum moment of inertia axis. Table 1 and Table 2 give the assumed parameters for asteroid Bennu and the spacecraft. We consider a frozen orbit with an initial semi-major axis of 1000 m; the initial conditions for the spacecraft are given in Table 3. The numerical simulation is carried out for 60 days, with a step size of 0.2 seconds. The differences in trajectories for the spacecraft assumed as a point mass and rigid body are illustrated in Figure 2. Figure 3 illustrates the spacecraft motion in the terminator plane. The trajectories shown are plotted in a frame rotating with the asteroid's motion around the Sun. As can be seen, the trajectory of the rigid body spacecraft rapidly diverges while the point mass spacecraft orbit remains frozen with respect to the Sun-asteroid line.

Table 1: Assumed parameters for asteroid 101955 Bennu (Chesley et al., 2014)

Parameter	Values
Mass	7.80×10^{10} kg
Size	$535 \times 565 \times 495$ m
Moment of Inertia	$10^{15} \times$ diag [2.138 2.013 2.294] kgm^2
Rotation Period	4.297 h
Obliquity	175°
Semi-major Axis	1.126 AU
Eccentricity	0.2037
Inclination	6.03°

Table 2: Spacecraft parameters

Parameter	Values
Mass	500 kg
Size	$0.9 \times 1.4 \times 1.8$ m
Moment of inertia	diag [216.66 168.75 115.4] kg-m^2
Reflectance coefficient	1
Spacecraft mass to area ratio	50 kg/m^2

Table 3: Initial conditions for relative states of spacecraft with respect to asteroid Bennu.

Parameter	Initial values
Relative position (m)	$\begin{bmatrix}100 & 0 & 945.2\end{bmatrix}^T$
Relative velocity (m/s)	$\begin{bmatrix}0 & -0.0751 & 0\end{bmatrix}^{\mathrm{T}}$
Relative attitude	$\mathrm{diag}\begin{bmatrix}1 & 1 & 1\end{bmatrix}$
Relative angular velocity (rad/s)	$\begin{bmatrix}0.02 & 0.08 & 0.0001\end{bmatrix}^T$

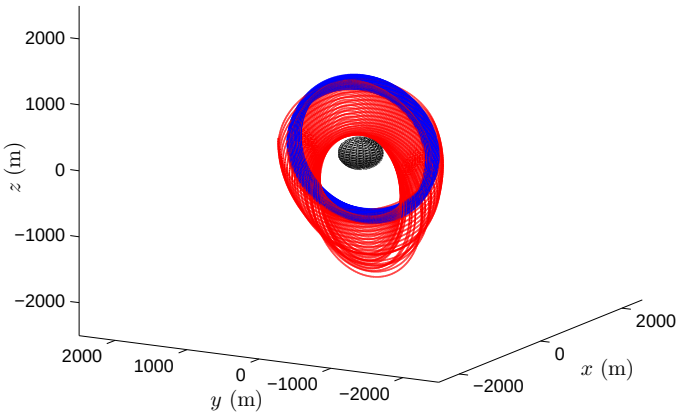

Figure 2: Frozen terminator orbit solution for asteroid Bennu. Red and blue trajectories represent rigid body and point mass motion respectively.

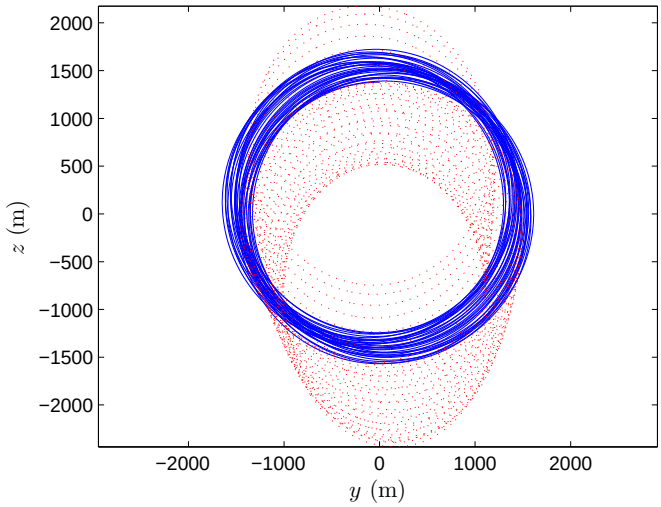

Figure 3: Trajectories shown in terminator YZ plane. Red and blue trajectories represent rigid body and point mass motion respectively.

5.3. Case II: 25143 Itokawa

In this subsection, spacecraft motion around 25143 Itokawa is analyzed using bounded initial conditions chosen randomly from a uniform distribution. Table 4 presents the parameters for the asteroid Itokawa. The spacecraft parameters considered are the same as discussed in the previous simulation, given in Table 2. Two numerical simulations are carried out, with and without the inclusion of SRP. The first numerical simulation is carried out for 25 days, with a step size of 0.1 seconds, and without the inclusion of SRP. Table 5 gives the initial conditions for the position and velocities of the spacecraft. The differences in trajectories for the spacecraft assumed as a point mass and rigid body are illustrated in Figure 4. We carry out another numerical propagation for 5 days with a step size of 0.1 seconds, this time including SRP in the model of the dynamics. The initial conditions for this simulation are given in Table 6. Figure 5 presents the trajectories for the point mass and rigid body model.

Table 4: Parameters for asteroid 25143 Itokawa (Fujiwara et al., 2006).

Parameter	Values
Mass	3.51×10^{10} kg
Size	$535 \times 294 \times 210$ m
Moment of Inertia	$10^{14} \times$ diag [2.336 5.912 6.670] kg-m^2
Rotation Period	12.132 h
Obliquity	178°
Semi-major Axis	1.323 AU
Eccentricity	0.280
Inclination	1.728°

Table 5: Initial conditions for pose and velocity of spacecraft for simulation illustrated in Figure 4.

Parameter	Initial values
Relative position (m)	$\begin{bmatrix} 0 & 800 & 0 \end{bmatrix}^T$
Relative velocity (m/s)	$\begin{bmatrix} 0 & -0.0219 & 0.0465 \end{bmatrix}^{\mathrm{T}}$
Relative attitude	$\mathrm{diag}\begin{bmatrix} 1 & 1 & 1 \end{bmatrix}$
Relative angular velocity (rad/s)	$\begin{bmatrix} 0.04 & 0.06 & 0.0005 \end{bmatrix}^T$

Table 6: Initial conditions for pose and velocity of spacecraft for simulation illustrated in Figure 5

Parameter	Values
Relative position (m)	Relative velocity (m/s)
$\begin{bmatrix} 150 & 800 & 0 \end{bmatrix}^T$	$\begin{bmatrix} 0 & 0.0271 & -0.0444 \end{bmatrix}^{\mathrm{T}}$
Relative attitude	Relative angular velocity (rad/s)
$\mathrm{diag}\begin{bmatrix} 1 & 1 & 1 \end{bmatrix}$	$\begin{bmatrix} 0.04 & 0.06 & 0.0005 \end{bmatrix}^T$

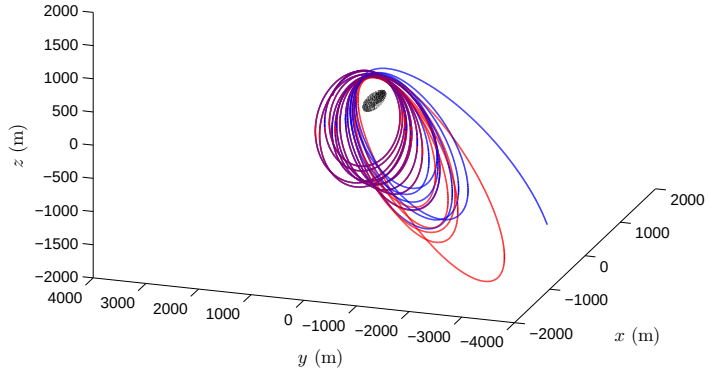

Figure 4: Spacecraft motion around asteroid Itokawa. Simulation has been carried out in the absence of SRP. Red and blue trajectories represent rigid body and point mass motion respectively.

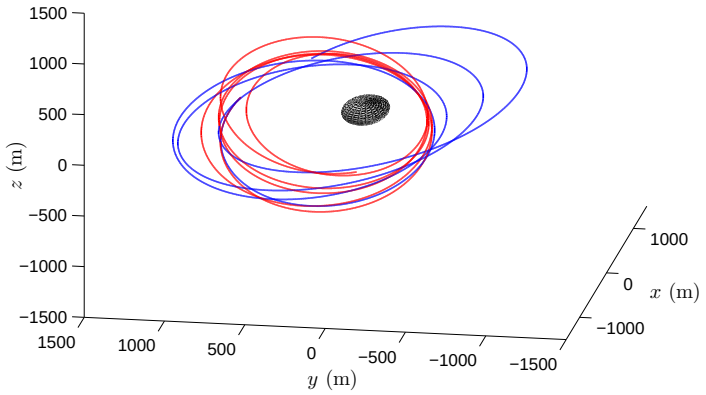

Figure 5: Spacecraft motion around asteroid Itokawa. Simulation has been carried out in the presence of SRP. Red, and blue trajectories represent rigid body and point mass motion respectively.

6. Implications of orbit-attitude coupling

Note that the spacecraft inertia and attitude-dependent terms that occur in the force on the spacecraft due to the asteroid's gravity, as given by eq (24), are up to an order of $\|r_c\|^{-4}$; this includes up to the second degree and order terms in the spherical harmonic expansion. Therefore, the attitude-dependent terms in this equation dominate over higher degree (degree > 2) terms obtained from the spherical harmonic expansion of the asteroid's gravity. In this regard, it is noteworthy that while high degree-and-order gravity field approximations for asteroids have been proposed and used based on spherical and ellipsoidal harmonic expansions (Takahashi et al., 2013; Garmier et al., 2002; Shi et al., 2012), the effects of the orbit-attitude coupling due to even the asteroid's primary gravity influence have not been considered during analysis of spacecraft missions to asteroids. A recent paper that considers the orbit-attitude (or translation-rotation) coupling for rigid spacecraft around spheroid planets is presented by Wang et al. (2012); however, they do not compare the trajectories obtained when this coupling is considered versus the traditional approach where the spacecraft is modeled

as a point mass for its translational motion. Furthermore the effects of solar gravity and SRP have not been considered in the paper.
As we show in the previous section, the spacecraft's trajectory is strongly influenced by this coupling over distances from the asteroid surface and time periods that are realistic for several upcoming or planned small-body missions. We expect that these qualitative differences between the traditional point mass model and the rigid body spacecraft model, and the strong influence of the orbit-attitude coupling on the spacecraft's trajectory, will remain when higher degree and order harmonic expansions for the asteroid's gravity field and its effects integrated over the spacecraft body are considered. While the effects of orbit-attitude coupling on the trajectory may be nullified by active control of the spacecraft, such control will require fuel expenditure that may not be necessary for exploration of the asteroid from orbit. More importantly, for model-based control near small Solar System bodies (asteroids and comets), using a model of the dynamics that accounts for this coupling will result in improved control performance and thereby fuel savings. This will require the model of the dynamics to account for orbit-attitude coupling, instead of using separate guidance, navigation and control schemes for orbital and attitude motions for such missions. Inclusion of orbit-attitude coupling in model of the dynamics could also lead to formulation of new control problems that utilize this coupling for small body exploration and hazard mitigation. An interesting foray in this direction is the study of underactuated spacecraft near small bodies using attitude actuation only. Besides, the asteroid's motion may be accurately estimated via remote sensing using the spacecraft's body-fixed sensors, as we describe in the following section.

7. Relative Pose Estimation

Consider a small solar system body in rotational and translational motion; the ranges (positions) and range rates (velocities) of a few points on its surface are observed by sensors fixed to a spacecraft in its proximity. Assume that the range and range rate of at least three points are observed, with optical sensors with known positions and line-of-sight directions in a coordinate frame fixed to the observing spacecraft.

7.1. Relative Pose Measurement Model

Let O denote the observed asteroid (or comet or space debris) and S denote the spacecraft. Let S denote a coordinate frame fixed to S and O be

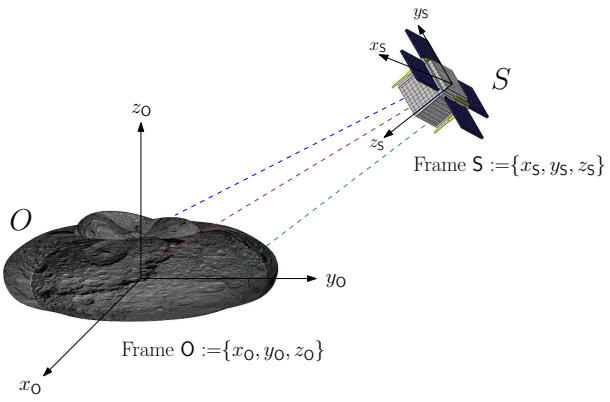

Figure 6: Small body O as observed from spacecraft S with optical measurements.

a coordinate frame fixed to O, as shown in Figure 6. During initialization, the frame axes of O and S could be chosen to be parallel. Let $Q \in \mathrm{SO}(3)$ be the relative rotation matrix from frame S to frame O and b denote the relative position of origin of S expressed in frame O. The pose (transformation) of frame S to frame O is

$$\mathsf{h} = \mathsf{g}_O^{-1}\mathsf{g}_S = \begin{bmatrix} Q & b \\ 0 & 1 \end{bmatrix} \in \mathrm{SE}(3), \tag{47}$$

where g_O and g_S denote asteroid's and spacecraft's pose, respectively. The positions of a set of feature points on space object O are observed by optical sensors fixed to spacecraft S. Velocities of these points are not directly measured, but may be calculated using a simple linear filter as in Izadi et al. (2015b). Assume that there are $n > 2$ feature points, which are always in the field-of-view (FOV) of the sensor fixed to spacecraft S, and the positions of these points are known in frame O as p_j, $j \in \{1, 2, \ldots, n\}$. These points generate $\binom{n}{2}$ unique pairwise relative position vectors, which are the vectors connecting any two of these points.

Denote the position of each optical sensor and the unit vector from that sensor to an observed point expressed in frame S as $s^k \in \mathbb{R}^3$ and $u^k \in \mathbb{S}^2, k = 1, \ldots, \mathsf{k}$, respectively. Denote the relative position of the j^{th} feature point observed by the k^{th} sensor expressed in frame S as q_j^k. Thus, in the absence of measurement noise

$$p_j = Q(q_j^k + s^k) + b = Qa_j + b, \; j \in \{1, 2, \ldots, n\}, \tag{48}$$

where $a_j = q_j^k + s^k$, are positions of these points expressed in S. In practice, the a_j are obtained from proximity optical measurements that will have additive noise; denote by a_j^m the measured vectors. In the case of lidar range measurements, these are given by

$$a_j^m = (q_j^k)^m + s^k = (\varrho_j^k)^m u^k + s^k,\ j \in \{1, 2, \ldots, n\}, \tag{49}$$

where $(\varrho_j^k)^m$ is the measured range to the point by the k^{th} sensor. The mean values of the vectors p_j and a_j^m are denoted as $\bar{p}$ and $\bar{a}^m$, and satisfy

$$\bar{p} = Q\bar{a}^m + b, \tag{50}$$

where $\bar{p} = \frac{1}{n}\sum_{j=1}^{n} p_j$ and $\bar{a}^m = \frac{1}{n}\sum_{j=1}^{n} a_j^m$. Consider the $\binom{n}{2}$ relative position vectors from optical measurements, denoted as $d_j = p_l - p_\ell$ in frame O and the corresponding vectors in frame S as $e_j = a_l - a_\ell$, for $l, \ell \in \{1, 2, \ldots, n\}$, $l \neq \ell$. Therefore,

$$d_j = Qe_j \Rightarrow D = QE, \tag{51}$$

where $D = [d_1\ \cdots\ d_n]$, $E = [e_1\ \cdots\ e_n] \in \mathbb{R}^{3\times n}$ with $n = \binom{n}{2}$. Note that the matrix of known relative vectors D is assumed to be known and bounded. Denote the measured value of matrix E in the presence of measurement noise as E^m. Then,

$$D = QE^m + \epsilon, \tag{52}$$

where $\epsilon \in \mathbb{R}^{3\times n}$ is the matrix of measurement errors in these vectors observed in frame S.

7.2. Relative Velocities Measurement Model

Denote the relative angular and translational velocity of object O expressed in body-fixed frame S by Ω and ν, respectively. Therefore, one can write the relative kinematics of spacecraft S w.r.t. object O as

$$\dot{Q} = Q\Omega^\times, \dot{b} = Q\nu \Rightarrow \dot{\mathsf{h}} = \mathsf{h}\xi^\vee, \tag{53}$$

where $\xi = \begin{bmatrix}\Omega \\ \nu\end{bmatrix} \in \mathbb{R}^6$ and $\xi^\vee = \begin{bmatrix}\Omega^\times & \nu \\ 0 & 0\end{bmatrix}$ and $(\cdot)^\times : \mathbb{R}^3 \to \mathfrak{so}(3) \subset \mathbb{R}^{3\times 3}$ is the skew-symmetric cross-product operator that gives the vector space

isomorphism between $\mathbb{R}^3$ and $\mathfrak{so}(3)$. In order to express relative velocities in terms of measurements, one can differentiate (48) as follows

$$\begin{aligned}
&\dot{p}_j = Q\Omega^{\times} a_j + Q\dot{a}_j + \dot{b} = Q\big(\Omega^{\times} a_j + \dot{a}_j + \nu\big) = 0 \\
\Rightarrow &\dot{a}_j - a_j^{\times}\Omega + \nu = 0 \\
\Rightarrow &v_j = \dot{a}_j = [a_j^{\times} \ -I]\xi = G(a_j)\xi,
\end{aligned} \tag{54}$$

where $G(a_j) = [a_j^{\times} \ -I]$ is a full rank matrix as long as vector a_j is nonzero (which is true for non-zero separation between the object and the spacecraft). From optical sensors, one can also obtain relative velocities of the observed points in frame S, denoted v_j^m. Here, velocity measurements as would be obtained by filtering position measurements or by optical flow is considered. The measurement model for velocities is

$$v_j^m = G(a_j)\xi + \vartheta_j, \tag{55}$$

where $\vartheta_j \in \mathbb{R}^3$ is the additive error in relative velocity measurement v_j^m. Instantaneous angular and translational velocity determination from such measurements is treated in Sanyal et al. (2014a). As $v_j = \dot{a}_j$ indicates, relative velocities of at least three points on O are needed to determine its relative translational and angular velocities uniquely at each instant. The relative velocities are obtained according to:

$$\mathbb{G}(A^m)\xi^m = \mathbb{V}(V^m) \Rightarrow \xi^m = \mathbb{G}^{\ddagger}(A^m)\mathbb{V}(V^m), \tag{56}$$

$$\text{where } \mathbb{G}(A^m) = \begin{bmatrix} G(a_1^m) \\ \vdots \\ G(a_n^m) \end{bmatrix} \text{ and } \mathbb{V}(V^m) = \begin{bmatrix} v_1^m \\ \vdots \\ v_n^m \end{bmatrix}, \tag{57}$$

are matrices consisting of position and velocity "measurements" from the optical sensor on spacecraft S and $\mathbb{G}^{\ddagger}(A^m) = \Big(\mathbb{G}^{\mathrm{T}}(A^m)\mathbb{G}(A^m)\Big)^{-1}\mathbb{G}^{\mathrm{T}}(A^m)$ is the pseudo-inverse of the full column rank matrix $\mathbb{G}(A^m)$.

7.3. Dynamic Estimation of Relative Motion from Proximity Measurements

To dynamically estimate relative motion states from optical measurements in close proximity, we apply the Lagrange-d'Alembert principle to an action functional of a Lagrangian of the relative motion estimate errors, with a

dissipation term linear in the relative velocities estimate error. Denote the estimated relative pose of the spacecraft as

$$\hat{\mathsf{h}} = \hat{\mathsf{g}}_O^{-1}\mathsf{g}_S = \begin{bmatrix} \hat{Q} & \hat{b} \\ 0 & 1 \end{bmatrix} \in \mathrm{SE}(3), \tag{58}$$

where $\hat{\mathsf{g}}_O$ denotes asteroid's estimated pose, and the relative pose estimation error as

$$\tilde{\mathsf{h}} = \mathsf{h}\hat{\mathsf{h}}^{-1} = \begin{bmatrix} \tilde{Q} & b - \tilde{Q}\hat{b} \\ 0 & 1 \end{bmatrix} = \begin{bmatrix} \tilde{Q} & x \\ 0 & 1 \end{bmatrix} \in \mathrm{SE}(3), \tag{59}$$

where $\tilde{Q} = Q\hat{Q}^{\mathrm{T}}$ is the relative attitude estimation error and $x = b - \tilde{Q}\hat{b}$. In the case of perfect measurements, one obtains

$$\dot{\tilde{\mathsf{h}}} = \tilde{\mathsf{h}}\varphi^{\vee}, \text{where } \varphi(\hat{\mathsf{h}}, \xi^m, \hat{\xi}) = \begin{bmatrix} \omega \\ \upsilon \end{bmatrix} = \mathrm{Ad}_{\hat{\mathsf{h}}}\big(\xi^m - \hat{\xi}\big), \tag{60}$$

and $\mathrm{Ad}_{\mathcal{g}} = \begin{bmatrix} \mathcal{R} & 0 \\ \mathcal{b}^{\times}\mathcal{R} & \mathcal{R} \end{bmatrix}$ for $\mathcal{g} = \begin{bmatrix} \mathcal{R} & \mathcal{b} \\ 0 & 1 \end{bmatrix}$. The relative attitude and position estimation error kinematics are

$$\dot{\tilde{Q}} = \tilde{Q}\omega^{\times}, \quad \dot{x} = \tilde{Q}\upsilon. \tag{61}$$

Consider a potential function as the sum of relative attitude and position measurement residuals between the measurements and estimates. Defining the trace inner product on $\mathbb{R}^{n_1 \times n_2}$ as

$$\langle A_1, A_2 \rangle := \mathrm{tr}(A_1^{\mathrm{T}} A_2), \tag{62}$$

one can define the relative attitude potential function as Wahba's cost function (Wahba, 1965)

$$\mathcal{U}_r^0(\hat{\mathsf{h}}, E^m, D) = \frac{1}{2}\langle D - \hat{Q}E^m, (D - \hat{Q}E^m)W \rangle, \tag{63}$$

where $W = \mathrm{diag}(w_j) \in \mathbb{R}^{n \times n}$ is a positive diagonal matrix of weight factors for the measured e_j^m and the relative position potential function

$$\begin{aligned} &\mathcal{U}_t(\hat{\mathsf{h}}, E^m) = \frac{1}{2}\kappa \|y(\hat{\mathsf{h}}, \bar{a}^m)\|^2, \text{ where} \\ &y(\hat{\mathsf{h}}, \bar{a}^m) = \bar{p} - \hat{Q}\bar{a}^m - \hat{b} \text{ and } \kappa > 0. \end{aligned} \tag{64}$$

The total potential function is defined as the sum of a generalized form of (63) used in Izadi and Sanyal (2014); Sanyal et al. (2014a) for attitude determination on SO(3), and the translational potential (64) as

$$\begin{aligned}\mathcal{U}(\hat{\mathsf{h}}, E^m, D) &= \Phi\big(\mathcal{U}_r^0(\hat{\mathsf{h}}, E^m, D)\big) + \mathcal{U}_t(\hat{\mathsf{h}}, E^m) \\ &= \Phi\big(\frac{1}{2}\langle D - \hat{Q}E^m, (D - \hat{Q}E^m)W\rangle\big) \\ &\quad + \frac{1}{2}\kappa\|\bar{p} - \hat{Q}\bar{a}^m - \hat{b}\|^2,\end{aligned} \tag{65}$$

where W is positive definite (not necessarily diagonal), and $\Phi : [0, \infty) \mapsto [0, \infty)$ is a $\mathcal{C}^2$ function that satisfies $\Phi(0) = 0$ and $\Phi'(\chi) > 0$ for all $\chi \in [0, \infty)$. Furthermore, $\Phi'(\cdot) \leq \alpha(\cdot)$ where $\alpha(\cdot)$ is a Class-$\mathcal{K}$ function (Khalil, 2001) and $\Phi'(\cdot)$ denotes the derivative with respect to the argument. Because of these properties of Φ, the critical points and their indices coincide for $\mathcal{U}_r^0$ and $\mathcal{U}_r$ (Izadi and Sanyal, 2014). Define the kinetic energy function

$$\mathcal{T}\Big(\varphi(\hat{\mathsf{h}}, \xi^m, \hat{\xi})\Big) = \frac{1}{2}\varphi(\hat{\mathsf{h}}, \xi^m, \hat{\xi})^{\mathrm{T}}\mathbb{J}\varphi(\hat{\mathsf{h}}, \xi^m, \hat{\xi}), \tag{66}$$

where $\mathbb{J} \in \mathbb{R}^{6\times 6} > 0$ is an artificial inertia-like kernel matrix. Note that in contrast to a rigid body's inertia matrix, $\mathbb{J}$ is not subject to intrinsic physical constraints (like triangle inequality, according to which the sum of any two eigenvalues of the inertia matrix is larger than the third) and is selected to tune the estimator. In order to simplify the expressions, we replace $\varphi(\hat{\mathsf{h}}, \xi^m, \hat{\xi})$ with φ from now on, although the dependence on the arguments exists. In the presence of measurement errors, we define the Lagrangian

$$\mathcal{L}(\hat{\mathsf{h}}, E^m, D, \varphi) = \mathcal{T}(\varphi) - \mathcal{U}(\hat{\mathsf{h}}, E^m, D), \tag{67}$$

and the corresponding action functional over an arbitrary time interval $[t_0, T]$ for $T > 0$,

$$\mathcal{S}\big(\mathcal{L}(\hat{\mathsf{h}}, E^m, D, \varphi)\big) = \int_{t_0}^{T} \mathcal{L}(\hat{\mathsf{h}}, E^m, D, \varphi)\mathrm{d}t, \tag{68}$$

such that $\dot{\hat{\mathsf{h}}} = \hat{\mathsf{h}}(\hat{\xi})^{\vee}$. In addition, using a Rayleigh dissipation term of the form $\mathbb{D}\varphi$ where $\mathbb{D} \in \mathbb{R}^{6\times 6} > 0$, and applying the Lagrange-d'Alembert principle from variational mechanics with *reduced variations* with respect to $\tilde{\mathsf{h}}$ and φ (Bloch et al., 2003; Marsden and Ratiu, 1999), yields the following estimator.

Theorem 7.1. *The nonlinear estimator for relative pose and velocities of a small-body with respect to a spacecraft in its proximity is*

$$\begin{cases} \mathbb{J}\dot{\varphi} & = \mathrm{ad}^*_{\varphi}\mathbb{J}\varphi - Z(\hat{\mathsf{h}}, E^m, D) - \mathbb{D}\varphi, \\ \dot{\hat{\xi}} & = \xi^m - \mathrm{Ad}_{\hat{\mathsf{h}}^{-1}}\varphi, \;\; \xi^m = \mathbb{G}^{\ddagger}(A^m)\mathbb{V}(V^m), \\ \dot{\hat{\mathsf{h}}} & = \hat{\mathsf{h}}(\hat{\xi})^{\vee}, \;\; \hat{\mathsf{g}}_O = \mathsf{g}_S\hat{\mathsf{h}}^{-1}, \end{cases} \tag{69}$$

where $\mathrm{ad}_{\zeta} = \begin{bmatrix} w^{\times} & 0 \\ v^{\times} & w^{\times} \end{bmatrix}$ *for* $\zeta = \begin{bmatrix} w \\ v \end{bmatrix}$, $\mathbb{G}, \mathbb{V}$ *are defined by* (57), $\mathrm{ad}^*_{\zeta} = (\mathrm{ad}_{\zeta})^T$ *and* $Z(\hat{\mathsf{h}}, E^m, D)$ *is defined by*

$$Z(\hat{\mathsf{h}}, E^m, D) = \begin{bmatrix} \Phi'\Big(\mathcal{U}^0_r(\hat{\mathsf{h}}, E^m, D)\Big) S_L(\hat{Q}) + \kappa\bar{p}^{\times} y(\hat{\mathsf{h}}, \bar{a}^m) \\ \kappa y(\hat{\mathsf{h}}, \bar{a}^m) \end{bmatrix}, \tag{70}$$

where $\mathcal{U}^0_r(\hat{\mathsf{h}}, E^m, D)$ *is defined as* (63), $y(\hat{\mathsf{h}}, \bar{a}^m) = \bar{p} - \hat{Q}\bar{a}^m - \hat{b}$ *and*

$$\begin{aligned} S_L(\hat{Q}) &= \mathrm{vex}\big(L\hat{Q}^T - \hat{Q}L^T\big) \\ &= \mathrm{vex}\big(DW(E^m)^T\hat{Q}^T - \hat{Q}E^m W D^T\big), \end{aligned} \tag{71}$$

$L = DW(E^m)^T$ *and* $\mathrm{vex}(\cdot) : \mathfrak{so}(3) \to \mathbb{R}^3$ *is the inverse of the* $(\cdot)^{\times}$ *map.*

This is a fundamentally new idea of applying a principle from variational mechanics to obtain a state estimator, recently employed in Izadi and Sanyal (2014). Prior work related to this idea, applying Hamilton-Jacobi-Bellman (HJB) theory (Kirk, 1971) to state estimation of rigid body attitude motion, appeared in Zamani (2013). This HJB formulation was "approximately solved" using an operator Riccati equation, to obtain a near-optimal filter. The performance of variational attitude estimator has been compared against those of some state-of-the-art filters in Izadi et al. (2015a).

7.4. Stability and Robustness of Estimator

The following result shows that the relative pose estimation scheme of Theorem 7.1 is stable, with almost global convergence of estimated states to real states for perfect measurements.

Theorem 7.2. *The estimator presented in Theorem 7.1 is asymptotically stable at the estimation error state* $(\tilde{\mathsf{h}}, \varphi) = (I, 0)$ *in the absence of measurement noise. Further, the domain of attraction of* $(\tilde{\mathsf{h}}, \varphi) = (I, 0)$ *is a dense open subset of* $\mathrm{SE}(3) \times \mathbb{R}^6$.

Proof: In the case of perfect measurements, $\hat{Q}E = \tilde{Q}^{\mathrm{T}}D$. Therefore,

$$\Phi\big(\mathcal{U}_r^0(\hat{\mathsf{h}}, E^m, D)\big) = \Phi\big(\mathcal{U}_r^0(\tilde{\mathsf{h}}, D)\big)$$

is a Morse function on SO(3). The stability of this estimator can be shown using the following candidate Morse-Lyapunov function, which can be interpreted as the total energy function corresponding to the Lagrangian (67):

$$\begin{aligned} V(\tilde{\mathsf{h}}, D, \varphi) &= \mathcal{T}(\varphi) + \mathcal{U}(\tilde{\mathsf{h}}, D) \\ &= \frac{1}{2}\varphi^{\mathrm{T}}\mathbb{J}\varphi + \Phi\big(\langle I - \tilde{Q}, K\rangle\big) + \frac{1}{2}\kappa y^{\mathrm{T}}y. \end{aligned} \tag{72}$$

Note that $V(\tilde{\mathsf{h}}, D, \varphi) \geq 0$ and $V(\tilde{\mathsf{h}}, D, \varphi) = 0$ if and only if $(\tilde{\mathsf{h}}, \varphi) = (I, 0)$. Therefore, $V(\tilde{\mathsf{h}}, D, \varphi)$ is positive definite on $\mathrm{SE}(3) \times \mathbb{R}^6$. Using (61), one can derive the time derivative of potential function $\mathcal{U}(\tilde{\mathsf{h}}, D)$ as

$$\begin{aligned} \frac{\mathrm{d}}{\mathrm{d}t}\mathcal{U}(\tilde{\mathsf{h}}, D) &= \Phi'(\mathcal{U}_r^0(\tilde{\mathsf{h}}, D))\big\langle -\tilde{Q}\omega^{\times}, K\big\rangle + \kappa(\dot{x} + \dot{\tilde{Q}}\bar{p})^{\mathrm{T}}(\tilde{Q}y) \\ &= \frac{1}{2}\Phi'(\mathcal{U}_r^0(\tilde{\mathsf{h}}, D))\big\langle \omega^{\times}, K\tilde{Q} - \tilde{Q}^{\mathrm{T}}K\big\rangle + \kappa(\upsilon + \omega^{\times}\bar{p})^{\mathrm{T}}y \\ &= \Phi'(\mathcal{U}_r^0(\tilde{\mathsf{h}}, D))S_K^{\mathrm{T}}(\tilde{Q})\omega + \kappa y^{\mathrm{T}}\upsilon + \kappa(\bar{p}^{\times}y)^{\mathrm{T}}\omega \\ &= Z^{\mathrm{T}}(\tilde{\mathsf{h}}, D)\varphi, \end{aligned} \tag{73}$$

where $S_K(\tilde{Q}) = \mathrm{vex}\big(K\tilde{Q} - \tilde{Q}^{\mathrm{T}}K\big)$ for $K = DWD^{\mathrm{T}}$, and $y = \tilde{Q}^{\mathrm{T}}x + (I - \tilde{Q}^{\mathrm{T}})\bar{p}$. Furthermore,

$$\begin{aligned} &Z(\tilde{\mathsf{h}}, D) = \\ &\begin{bmatrix} \Phi'\Big(\big\langle I - \tilde{Q}, K\big\rangle\Big)S_K(\tilde{Q}) + \kappa\bar{p}^{\times}\big\{\tilde{Q}^{\mathrm{T}}x + (I - \tilde{Q}^{\mathrm{T}})\bar{p}\big\} \\ \kappa\{\tilde{Q}^{\mathrm{T}}x + (I - \tilde{Q}^{\mathrm{T}})\bar{p}\} \end{bmatrix}. \end{aligned} \tag{74}$$

Hence, the time derivative of the candidate Morse-Lyapunov function is

$$\begin{aligned} \dot{V}(\tilde{\mathsf{h}}, D, \varphi) &= \varphi^{\mathrm{T}}\mathbb{J}\dot{\varphi} + \varphi^{\mathrm{T}}Z(\tilde{\mathsf{h}}, D) \\ &= \varphi^{\mathrm{T}}\Big(\mathrm{ad}_{\varphi}^{*}\mathbb{J}\varphi - Z(\tilde{\mathsf{h}}, D) - \mathbb{D}\varphi + Z(\tilde{\mathsf{h}}, D)\Big) = -\varphi^{\mathrm{T}}\mathbb{D}\varphi. \end{aligned} \tag{75}$$

noting that $\varphi^{\mathrm{T}}\mathrm{ad}^*_{\varphi}\mathbb{J}\varphi = 0$ and

$$\mathbb{J}\dot{\varphi} = \mathrm{ad}^*_{\varphi}\mathbb{J}\varphi - Z(\tilde{\mathsf{h}}, D) - \mathbb{D}\varphi, \tag{76}$$

in the absence of measurement noise. Hence, the derivative of the Morse-Lyapunov function is negative semi-definite. Note that the dynamics of the relative pose estimate error $\tilde{\mathsf{h}}$ is given by (60), while dynamics of the relative velocities estimate error φ is given by (76). Therefore, the error dynamics for $(\tilde{\mathsf{h}}, \varphi)$ is non-autonomous, as they depend explicitly on measurements D. Considering (72) and (75) and applying Theorem 8.4 in Khalil (2001), one can conclude that $\varphi^{\mathrm{T}}\mathbb{D}\varphi \to 0$ as $t \to \infty$, which consequently implies $\varphi \to 0$. Thus, the positive limit set for this system is contained in

$$\mathcal{E} = \dot{V}^{-1}(0) = \big\{(\tilde{\mathsf{h}}, \varphi) \in \mathrm{SE}(3) \times \mathfrak{se}(3) : \varphi \equiv 0\big\}. \tag{77}$$

Substituting $\varphi \equiv 0$ in the first equation of (69), we obtain the positive limit set where $\dot{V} \equiv 0$ (or $\varphi \equiv 0$) as the set

$$\begin{aligned} \mathscr{I} &= \big\{(\tilde{\mathsf{h}}, \varphi) \in \mathrm{SE}(3) \times \mathbb{R}^6 : Z(\tilde{\mathsf{h}}, D) \equiv 0, \varphi \equiv 0\big\} \\ &= \big\{(\tilde{\mathsf{h}}, \varphi) \in \mathrm{SE}(3) \times \mathbb{R}^6 : \tilde{Q} \in C_{\tilde{Q}},\ \tilde{Q}^{\mathrm{T}}x = 0,\ \varphi \equiv 0\big\}. \end{aligned} \tag{78}$$

Therefore, for perfect measurement errors, all solutions of this estimator converge asymptotically to the set $\mathscr{I}$. Define $\mathcal{U}_r(\tilde{Q}) := \Phi\big(\langle I - \tilde{Q}, K\rangle\big)$, which is the attitude measurement residual in the case of perfect measurements. Thus, the relative attitude estimate error converges to the set of critical points of $\mathcal{U}_r(\tilde{Q})$ in this intersection, and the relative position estimate error x converges to zero. The unique global minimum of $\mathcal{U}_r(\tilde{Q})$ is at $\tilde{Q} = I$ (Lemma 2.1 in Izadi and Sanyal (2014)), so this estimation error is asymptotically stable.

Now consider the set

$$\mathscr{C} = \mathscr{I} \setminus (I, 0), \tag{79}$$

which consists of all stationary states that the estimation errors may converge to, besides the desired estimation error $(I, 0)$. Note that all states in the stable manifold of a stationary state in $\mathscr{C}$ converge to this stationary state. From the properties of the critical points $\tilde{Q}_\iota \in C_{\tilde{Q}} \setminus (I)$ of $\mathcal{U}^0_r(\tilde{Q})$, $(\iota = 1, 2, 3)$ given in Lemma 2.1 of Izadi and Sanyal (2014), we see that the stationary points in $\mathscr{I} \setminus (I, 0) = \big\{(\begin{bmatrix} \tilde{Q}_\iota & 0 \\ 0 & 1 \end{bmatrix}, 0) : \tilde{Q}_\iota \in C_{\tilde{Q}} \setminus (I)\big\}$ have stable manifolds

whose dimensions depend on the index of $\tilde{Q}_\iota$. Since the velocities estimate error φ converges globally to the zero vector, the dimension of the stable manifold $\mathcal{M}_\iota^S$ of the critical points, i.e. $(\begin{bmatrix}\tilde{Q}_\iota & 0\\ 0 & 1\end{bmatrix}, 0) \in \mathrm{SE}(3) \times \mathbb{R}^6$ is

$$\dim(\mathcal{M}_\iota^S) = 9 + (3 - \text{ index of } \tilde{Q}_\iota) = 12 - \text{ index of } \tilde{Q}_\iota. \tag{80}$$

Therefore, the stable manifolds of $(\tilde{\mathsf{h}}, \varphi) = (\begin{bmatrix}\tilde{Q}_\iota & 0\\ 0 & 1\end{bmatrix}, 0)$ are nine-dimensional, ten-dimensional, or eleven-dimensional, depending on the index of $\tilde{Q}_\iota \in C_{\tilde{Q}} \setminus (I)$ according to (80). Moreover, the value of the Lyapunov function $V(\tilde{\mathsf{h}}, D, \varphi)$ is non-decreasing (increasing when $(\tilde{\mathsf{h}}, \varphi) \notin \mathscr{I}$) for trajectories on these manifolds when going backwards in time. This implies that the metric distance between error states $(\tilde{\mathsf{h}}, \varphi)$ along these trajectories on the stable manifolds $\mathcal{M}_\iota^S$ grows with the time separation between these states, and this property does not depend on the choice of the metric on $\mathrm{SE}(3) \times \mathbb{R}^6$. Therefore, these stable manifolds are embedded (closed) submanifolds of $\mathrm{SE}(3) \times \mathbb{R}^6$ and so is their union. Clearly, all states starting in the complement of this union, converge to the stable equilibrium $(\begin{bmatrix}\tilde{Q}_\iota & 0\\ 0 & 1\end{bmatrix}, 0) = (I, 0)$; therefore the domain of attraction of this equilibrium is

$$\mathrm{DOA}\{(I,0)\} = \mathrm{SE}(3) \times \mathbb{R}^6 \setminus \big\{ \cup_{\iota=1}^3 \mathcal{M}_\iota^S \big\},$$

which is a dense open subset of $\mathrm{SE}(3) \times \mathbb{R}^6$. □

Thus, for perfect measurements, the domain of attraction of this variational estimation scheme at $(\tilde{\mathsf{h}}, \varphi) = (I, 0)$ is almost global over the state space $\mathrm{TSE}(3) \simeq \mathrm{SE}(3) \times \mathbb{R}^6$. This is the best that one can do with continuous schemes for state estimation or control for systems evolving on non-contractible state spaces (Chaturvedi et al., 2011; Milnor, 1963). In the presence of unbiased measurements with stochastic noise, the expected values of the state estimates can be shown to converge to the true states.

8. Conclusion

This work presents several new results in the topic of spacecraft exploration of small Solar System bodies. The two primary results are: (1) a more accurate model of the dynamics than has been considered in the literature so far, which shows that the spacecraft dynamics in proximity to a small body

deviates from the dynamics of a point mass; and (2) a (relative) motion estimation scheme for estimating the motion of the small body using vision-based measurements that does not require any knowledge of dynamics of the body. The first result is a significant contribution to small body proximity missions, which have hitherto considered the spacecraft in proximity to the body (asteroid or comet) to be modeled by a point mass for its trajectory about the body. A rigorous analysis shows that the attitude of the spacecraft affects its trajectory through dynamical coupling, as the weak gravity force on the spacecraft due to the small body is dependent on the spacecraft's attitude. Moreover, this dependency is stronger than higher-order gravity terms arising from a harmonic expansion of the gravity force field; it is noteworthy that these higher order terms have been considered in past research while the more influential attitude-dependent gravity terms have been neglected. The second main contribution of this work is a relative motion estimation scheme that can estimate the relative pose and velocities of the small body, based on vision sensor measurements onboard the spacecraft. Assuming that the spacecraft has knowledge of its own pose and velocities in a heliocentric inertial frame (which is a reasonable assumption), this estimation scheme therefore gives the absolute pose and velocities of the small body in this inertial frame. Moreover, it does not require any knowledge of the dynamics of the small body, which is particularly advantageous for exploration of newly discovered small bodies in the Solar System.

Acknowledgement

The authors acknowledge funding for this research through NSF grant CMMI 1131643 and NASA grant NNX11AQ35A. Suggestions and comments from the anonymous reviewers and from Dr. Carlos Roithmayr of NASA Langley Research Center that helped improve this manuscript, are also gratefully acknowledged.

References

Beck, J., Hall, C., 1998. Relative equilibria of a rigid satellite in a circular Keplerian orbit. Journal of the Astronautical Sciences 46 (3), 215–247.

Bloch, A., Ballieul, J., Crouch, P., Marsden, J., 2003. Nonholonomic Mechanics and Control, Volume 24 of Interdisciplinary Applied Mathematics. Springer-Verlag, New York.

Broschart, S., 2006. Close proximity spacecraft maneuvers near irregularly shaped small bodies; hovering, translation, and descent. Ph.D. thesis, University of Michigan, Ann Arbor, MI.

Chaturvedi, N., Sanyal, A., McClamroch, N., 2011. Rigid-body attitude control. Control Systems Magazine, IEEE 31 (3), 30–51.

Chesley, S., Farnocchia, D., Nolan, M., Vokrouhlickỳ, D., Chodas, P., Milani, A., Spoto, F., Rozitis, B., Benner, L., Bottke, W., et al., 2014. Orbit and bulk density of the OSIRIS-REx target asteroid (101955) Bennu. Icarus 235, 5–22.

Fruh, C., Jah, M., Kelcey, T., 2013. Coupled orbit-attitude dynamics of high area-to-mass ratio (HAMR) objects: Influence of solar radiation pressure, Earth's shadow and the visibility in light curves. Celestial Mechanics and Dynamical Astronomy 117, 385–404.

Fujiwara, A., Kawaguchi, J., Yeomans, D., Abe, M., Mukai, T., Okada, T., Saito, J., Yano, H., Yoshikawa, M., Scheeres, D., et al., 2006. The rubble-pile asteroid Itokawa as observed by Hayabusa. Science 312 (5778), 1330–1334.

Garmier, R., Barriot, J., Konopliv, A., Yeomans, D., 2002. Modeling of the Eros gravity field as an ellipsoidal harmonic expansion from the NEAR Doppler tracking data. Geophysical Research Letters 29 (8), 72–1–72–3.

Giancotti, M., 2014. Stable orbits in the proximity of an asteroid: Solutions for the Hayabusa-2 mission. Ph.D. thesis, Università di Roma La Sapienza, Rome, Italy.

Hairer, E., Lubich, C., Wanner, G., 2002. Geometric Numerical Integration. Springer Verlag, New York.

Harris, A., Barucci, M., Cano, J., Fitzsimmons, A., Fulchignoni, M., Green, S., Hestroffer, D., Lappas, V., Lork, W., Michel, P., Morrison, D., Payson, D., Schaeffer, F., 2013. The European union funded NEOSHIELD project: A global approach to near-Earth object impact threat mitigation. Acta Astronautica 90 (1), 80–84.

Hu, W., 2002. Orbital motion in uniformly rotating second degree and order gravity fields. Ph.D. thesis, University of Michigan, Ann Arbor, MI.

Hu, W., Scheeres, D., 2002. Spacecraft motion about slowly rotating asteroids. Journal of Guidance, Control and Dynamics 25 (4), 765–775.

Hussein, I., Leok, M., Sanyal, A., Bloch, A., 2006. A discrete variational integrator for optimal control problems in SO(3). In: Proceeding of the 45th IEEE Conference on Decision and Control. San Diego, CA, pp. 6636–6641.

Izadi, M., Samiei, E., Sanyal, A., Kumar, V., 2015a. Comparison of an attitude estimator based on the Lagrange-d'Alembert principle with some state-of-the-art filters. In: Proceeding of the IEEE International Conference on Robotics and Automation, May 26 - 30. Seattle, WA.

Izadi, M., Sanyal, A., 2014. Rigid body attitude estimation based on the Lagrange-d'Alembert principle. Automatica 50 (10), 2570 – 2577.

Izadi, M., Sanyal, A., Samiei, E., Viswanathan, S., 2015b. Discrete-time rigid body attitude state estimation based on the discrete Lagrange-d'Alembert principle. In: Proceeding of the American Control Conference, July 1 - 3. Chicago, IL.

Khalil, H., 2001. Nonlinear Systems, 3rd Edition. Prentice Hall, Upper Saddle River, NJ.

Kirk, D., 1971. Optimal Control Theory: An Introduction. Prentice Hall, New York.

Koon, W., Marsden, J., Ross, S., Lo, M., Scheeres, D., 2004. Geometric mechanics and the dynamics of asteroid pairs. Annals of the New York Academy of Sciences 1017, 11–38.

Lee, T., Leok, M., McClamroch, N., 2007. Lie group variational integrators for the full two body problem in orbital mechanics. Celestial Mechanics and Dynamical Astronomy 98, 121–144.

Lu, E., Love, S., 2005. Gravitational tractor for towing asteroids. Nature 438, 177–178,.

Marsden, J., Ratiu, T., 1999. Introduction to Mechanics and Symmetry: A Basic Exposition of Classical Mechanical Systems, 2nd Edition. Vol. 17. Springer Science & Business Media.

Marsden, J., West, M., 2001. Discrete mechanics and variational integrators. Acta Numerica 10, 357–514.

Mazanek, D., Brophy, J., Merrill, R., 2013. Asteroid retrieval mission concept: Trailblazing our future in space and helping to protect us from Earth impactors. In: IAA Planetary Defense Conference, April 15-19. Flagstaff, AZ.

Mignard, F., Hènon, M., 1984. About an unsuspected integrable problem. Celestial Mechanics and Dynamical Astronomy 33, 239–250.

Miller, J., Konopliv, A., Antreasian, P., Bordi, J., Chesley, S., Helfrich, C., Owen, W., Wang, T., Williams, B., Yeomans, D., et al., 2002. Determination of shape, gravity, and rotational state of asteroid 433 Eros. Icarus 155 (1), 3–17.

Milnor, J., 1963. Morse Theory. Princeton University Press, Princteon, New Jersey.

Mohan, S., Breakwell, J., Lange, B., 1972. Interaction between attitude libration and orbital motion of a rigid body in a near Keplerian orbit of low eccentricity. Celestial Mechanics 5, 157–173.

Monforte, J., 2002. Geometric, Control and Numerical Aspects of Nonholonomic Systems. No. 1793. Springer-Verlag, Berlin-Heidelberg.

Nordkvist, N., Sanyal, A., 2010. A Lie group variational integrator for rigid body motion in SE(3) with applications to underwater vehicles. In: Proceeding of the 49th IEEE Conference on Decision and Control. Atlanta, GA, pp. 5414–5419.

Pan, H., Kapila, V., 2001. Adaptive and nonlinear control for spacecraft formation flying with coupled translational and attitude dynamics. In: Proceeding of the 40th IEEE Conference on Decision and Control. Orlando, FL.

Pascal, M., 1985. Numerical investigation of all possible equilibria of dual spin satellites. Celestial Mechanics 37 (1), 81–93.

Prado, J., Perret, A., Boisard, O., 2011. Deflecting Apophis with a flotilla of solar shields. Advances in Space Research 48 (11), 1911–1916.

Russell, C., Raymond, C., Coradini, A., McSween, H., Zuber, M., Nathues, A., Sanctis, M. D., Jaumann, R., Konopliv, A., Preusker, F., et al., 2012. Dawn at Vesta: Testing the protoplanetary paradigm. Science 336 (6082), 684–686.

Sanyal, A., 2004. Dynamics and control of multibody systems in central gravitational field. Ph.D. thesis, University of Michigan, Ann Arbor, MI.

Sanyal, A., Izadi, M., Butcher, E., 2014a. Determination of relative motion of a space object from simultaneous measurements of range and range rate. In: Proceeding of the American Control Conference, June 4 - 6. Portland, OR, pp. 1607–1612.

Sanyal, A., Izadi, M., Misra, G., Samiei, E., Scheeres, D., 2014b. Estimation of dynamics of space objects from visual feedback during proximity operations. In: AIAA/AAS Astrodynamics Specialist Conference, July 18. San Diego, CA.

Schaub, H., Junkins, J., 2009. Analytical Mechanics of Space Systems. American Institute of Aeronautics and Astronautics, Reston, VA.

Scheeres, D., 1994. Dynamics about uniformly rotating triaxial ellipsoids: Application to asteroids. Icarus 110, 225–238.

Scheeres, D., 1999. Satellite dynamics about small bodies: Averaged solar radiation pressure effects. Journal of the Astronautical Sciences 47 (1), 25–46.

Scheeres, D., 2012a. Orbital mechanics about small bodies. Acta Astronautica 72 (2), 1–14.

Scheeres, D., 2012b. Orbital Motion in Strongly Perturbed Environments. Springer, Berlin-Heidelberg.

Scheeres, D., Fahnestock, E., Ostro, S., Margot, J., Benner, L., Broschart, S., Bellerose, J., Giorgini, J., Nolan, M., Magri, C., Pravec, P., Scheriech, P., Rose, R., Jurgens, R., Jong, E. D., Suzuki, S., 2006. Dynamical configuration of binary Near-Earth Asteroid (66391) 1999 KW4. Science 314 (5803), 1280–1283.

Scheeres, D., Sutter, B., Rosengren, A., 2013. Design, dynamics and stability of the OSIRIS-REx Sun-Terminator orbits. In: Proceeding of the 23rd AAS/AIAA Spaceflight Mechanics Meeting. Kauai. HI.

Segal, S., Gurfil, P., 2009. Effects of kinematic rotation-translation coupling on relative spacecraft translation dynamics. Journal of Guidance, Control and Dynamics 32, 1045–1050.

Shi, X., Willner, K., Oberst, J., Ping, J., Ye, S., 2012. Working models for the gravity field of Phobos. Science China Physics, Mechanics and Astronomy 91 (2), 358–364.

Sincarsin, G., Hughes, P., 1983. Gravitational orbit-attitude coupling for very large spacecraft. Celestial Mechanics 31 (2), 143–161.

Takahashi, Y., Scheeres, D., 2011. Small-body postrendezvous characterization via slow hyperbolic flybys. Journal of Guidance, Control, and Dynamics 34 (6), 1815–1827.

Takahashi, Y., Scheeres, D., Werner, R., 2013. Surface gravity fields for asteroids and comets. AIAA Journal of Guidance, Control, and Dynamics 36 (2), 362–374.

Tsuda, Y., Yoshikawa, M., Abe, M., Minamino, H., Nakazawa, S., 2013. System design of the Hayabusa-2- asteroid sample return mission to 1999JU3. Acta Astronautica 91, 356–362.

Vasile, M., Maddock, C., 2012. Design of a formation of solar pumped lasers for asteroid deflection. Advances in Space Research 50 (7), 891–905.

Wahba, G., 1965. A least squares estimate of satellite attitude, Problem 65-1. SIAM Review 7 (5), 409.

Wang, Y., Xu, S., Zhu, M., 2012. Gravitational orbit-rotation coupling of a rigid satellite around a spheroid planet. Journal of Aerospace Engineering 27 (1), 140–150.

Yu, Y., Baoyin, H., 2012. Orbital dynamics in the vicinity of asteroid 216 Kleopatra. Astronomical Journal 143 (2), 62–70.

Zamani, M., 2013. Deterministic attitude and pose filtering, an embedded Lie groups approach. Ph.D. thesis, Australian National University, Canberra, Australia.